Ultrabroadband Diode-Like Asymmetric Transmission and High-Efficiency Cross-Polarization Conversion Based on Composite Chiral Metamaterial

Yongzhi Cheng[1, *], Jingcheng Zhao[2], Xuesong Mao[1], and Rongzhou Gong[3]

Abstract—In this paper, a three layer composite chiral metamaterial (CCMM) is proposed to achieve diode-like asymmetric transmission and high-efficiency cross-polarization conversion by 90° polarization rotation with ultrabroadband range in microwave region, which was verified by simulation and experiment. This CCMM is composed of a disk-split-ring (DSR) structure sandwiched between two twisted sub-wavelength metal grating structures. The simulation agrees well with experiment in principle. The simulation results indicate that the incident $y(x)$-polarized wave propagation along the $-z(+z)$ direction through the CCMM slab is still linearly polarized wave with high purity, but the polarization direction is rotated by $\pm 90°$, and the polarization conversion ratio (PCR) is greater than 90% in the frequency range of 4.36–14.91 GHz. In addition, in the above frequency range, the asymmetric transmission coefficient (Δ_{lin}) and the total transmittance (T_x) for x-polarized wave propagation along the $-z$ axis direction are both over 0.8. Finally, the above experiment and simulation results were further verified by the electric field distribution characteristics of the CCMM unit-cell structure. Our design will provide an important reference for the practical applications of the CCMM for polarization manipulation.

1. INTRODUCTION

Chiral metamaterial (CMM) is an important subset of metamaterials (MMs), the unit-cell structure of which cannot be superimposed onto its mirror image [1–8], resulting in a cross-coupling effect of the electric and magnetic field. Since the mirror symmetry of unit-cell is broken either in the perpendicular plane or in the propagation direction, numerous outstanding electromagnetic (EM) properties of the CMMs can be achieved, such as negative refraction [3–8], giant optical activity [6, 7, 9] and circular dichroism [8, 10], asymmetric transmission (AT) effect [11–15], and polarization conversion or rotation [16–19]. Especially, manipulating and controlling the polarization property of EM waves using CMMs is of central interest, which also attracts great attention increasingly [16–28]. The AT effect was firstly observed and demonstrated by Fedotov et al. in 2006 [11], which is one of the most remarkable applications of CMMs [29–46]. The AT effect, as a novel phenomenon for the CMMs, originates from the difference in total cross-polarized transmission waves propagating in two opposite directions [12]. It is similar to electronic diode effect that can block the electric current in one direction while allowing it to flow through the diode in the opposite direction. The AT effect is irrelevant to the nonreciprocity of the Faraday effects, which can happen in the absence of magneto-optical media [13–15]. Essentially, the AT effect rigorously obeys Lorentz's reciprocity [33], which can be explained by de Hoop reciprocity

[1] School of Information Science and Engineering, Wuhan University of Science and Technology, Wuhan, Hubei 430081, China. [2] School of Electronics and Information Engineering, Beihang University, Beijing 100191, China. [3] School of Optical and Electronic Information, Huazhong University of Science and Technology, Wuhan 430074, China.

and described using the Jones matrix [14, 15]. AT is very useful in realizing diode-like effect and EM polarization manipulation devices such as isolators and polarization convertors [34–37].

Hence, the AT effect of circular and linear polarization waves has being extensively studied, and various CMM structures have been proposed and demonstrated from microwave to optical frequency range [29–46]. At early stage, a bi-layered CMM in the near-infrared region was proposed and demonstrated by Menzel et al., which could achieve only a magnitude of 0.25 for linear polarization waves with a single band [29]. Then, Kang et al. theoretically demonstrated that a special CMM breaking the symmetry in the propagation direction could realize the AT effect for linear polarization wave, and the magnitude of AT parameter could achieve 0.45 [30]. However, it could only work with a single band. Subsequently, a thin CMM combined with the EM wave tunneling was proposed, which could realize a near unity magnitude of AT parameter with a dual-band [33]. After that, an increasing number of CMM structures for AT effects of circular and linear polarization waves have been proposed [34–43], some of which have enriched functionality, such as high cross-polarization conversion (CPC) efficiency, multiband and broadband operation frequency. However, most of these CMMs for AT effect do not have a broad bandwidth and high CPC simultaneously, which restricts their applications in many fields. More recently, tri-layer structures based on Fabry-Perot-like resonance were proposed by Liu et al. [42], and the operation bandwidth could be extended to some degree [44–47]. However, up to now, the composite CMM with ultrabroadband as well as near unity CPC efficiency (the relative bandwidth of over 90% CPC efficiency is greater than 90%) has not been achieved. In addition, the thickness of these composite CMM structure samples is usually large, and the CPC efficiency is relatively low, which is inconvenient in some practical applications, especially in radio and even microwave frequency range.

To ours best knowledge, nearly all of the proposed MM structures with the AT effect and CPC usually operate in a low magnitude or a relative narrow frequency range [14–20, 29–46]. Thus, the high magnitude and broadband in MMs for cross-polarization conversion and AT effect are still desirable. In this work, ultra-broadband diode-like AT effect for linear polarization waves and high-efficient CPC in a tri-layer CCMM are proposed and demonstrated numerically and experimentally. The simulation results show the CPC and diode-like AT effect for linearly polarized waves in an ultra-broadband frequency range of 4.36–14.91 GHz, where polarization conversion ratio (PCR) is greater than 95%, which agrees well with experiment. The corresponding relative bandwidth of our design can be extended extremely and up to 109.49%, which is remarkable compared with the previous CMM structures [29–43].

2. UNIT-CELL STRUCTURE DESIGN, SIMULATION AND EXPERIMENT

Figure 1 shows the design schematics of the CCMM, which consists of a disk-split-ring structure (DSRs) sandwiched with two twisted sub-wavelength metal grating structure. As shown in Fig. 1(d), we decompose the unit-cell structure of the CCMM into three functional components: layer A, layer B and layer C, and layers AB and BC are separated by a dielectric spacer layer. Layer A and layer C can be functioned as a polarization selector, and the special polarized (e.g., x-polarized) wave can be allowed to pass through it, but the other polarized (e.g., y-polarized) wave will be blocked significantly [42, 46, 47]. Layer B can be served as a polarization convertor. The DSRs of layer B have been proposed and investigated [49, 50], which behave as a dipole resonator and couple a special electric field component of the incident EM wave, finally resulting in a partial polarization conversion in a broadband range. Thus, it gives us an idea using the DSRs as the middle layer resonator structure in design of the CCMM for broadband high-efficient CPC and AT effect. The front (layer A) and back (layer C) grating structures are geometrically identical but are twisted an angle of 90° in x-y plane to generate the strong chirality due to the near-field electric and magnetic cross-coupling effect. In this design, the middle split direction of the DSRs is rotated 45° along $x(y)$ axis. Thus, an asymmetry is introduced in the unit-cell structure so that it has no line of mirror symmetry, enabling the AT effect only for linear polarization wave. Similar to previous designs [46, 47, 51], the multi-layered structure of the proposed CCMM can form a Fabry-Perot-like cavity, which could realize a multi-band or broadband AT effect due to the superposition of multiple reflections and transmission, and the mirror symmetry breaking along the propagation direction. The optimized geometry parameters are as follow: $p_x = p_y = 9$ mm, $d = 1.5$ mm, $g_1 = 0.9$ mm, $r_1 = 4.3$ mm, $r_0 = 1.3$ mm, $w = 1.2$ mm, $g_2 = 2.3$ mm, $t_s = 2.5$ mm, $t_m = 35$ μm.

To study its eciency and gain insight into the physical mechanism of the AT effect and CPC, the
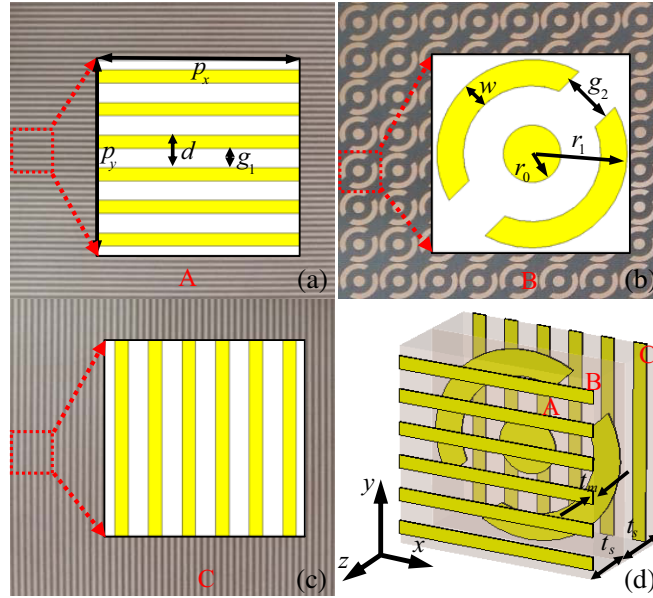
Figure 1. The schematic diagram and portion photograph of the tested sample of the designed CCMM: (a), (b), (c) are the schemes of the front, middle and bottom layer structure and the corresponding portion photograph of the tested sample; (d) perspective view of the unit-cell structure.

finite integration technique (FIT) simulations are performed by using the frequency domain solver of the CST Microwave Studio. In simulation, the periodic boundary conditions were applied to the x and y directions of the unit-cell structure while the open boundary conditions are set at z sides. The metallic structure layers were modeled as a copper film with an electric conductivity $\sigma = 5.8 \times 10^7$ S/m. We selected low loss dielectric substrate Rogers RO4003 as the isotropic spacer layer, and the relative permittivity is $\varepsilon_r = 2.75(1 + 0.0027i)$.

To further verify its efficiency experimentally, the designed CCMM was fabricated into a 22×22 unit-cell sample by the conventional printed circuit board (PCB) process according to the optimized geometric parameters. In fabrication process, layer A and layer B metallic structures were printed on both sides of the blank Rogers RO4003 board, and layer C was printed on one side of the blank Rogers RO4003 board. Then, B plane and blank plane of C layer of the two printed boards are glued closely together using an adhesive with 0.03 mm thickness. Finally, the total dimension of the fabricated CCMM slab is about 198 mm × 198 mm × 5.1 mm. The measurements of the fabricated CCMM sample were carried out in an EM anechoic chamber. The two broadband horn antennas connected to a vector network analyzer (Agilent PNA-X N5244A) by coaxial cable are used to measure the complex transmission coefficients from 3 to 17 GHz. In measurement, the CCMM slab is placed in the middle position of the horn antennas, which are distributed by a distance of 1.5 m to eliminate the near-field effect [16, 18, 51]. The plane waves with y- and x-polarizations are generated and received by rotating the orientation of the two horn antennas [52].

3. THE RESULTS AND DISCUSSIONS

We firstly study the responses of the single layer B bi-layer AB and bi-layer BC, respectively. Fig. 2(a) shows the simulated transmission coefficients of the single layer B for the normal incident waves propagation along backward $(-z)$ direction. It can be seen that the two cross-polarization transmission coefficients (t_{xy}^b and t_{yx}^b) are the same, and the magnitudes are up to maximal values of 0.51 and 0.64 at 10.51 GHz and 14.88 GHz, respectively. At the meantime, the two co-polarization transmission coefficients (t_{xx}^b and t_{yy}^b) are also the same, and the magnitudes are decreased to 0.33 and 0.53 at 9.25 GHz and 14.88 GHz, respectively. It means that the single DSR can convert a linearly polarized wave partially to its orthogonal component within a broadband frequency range. To get insight into
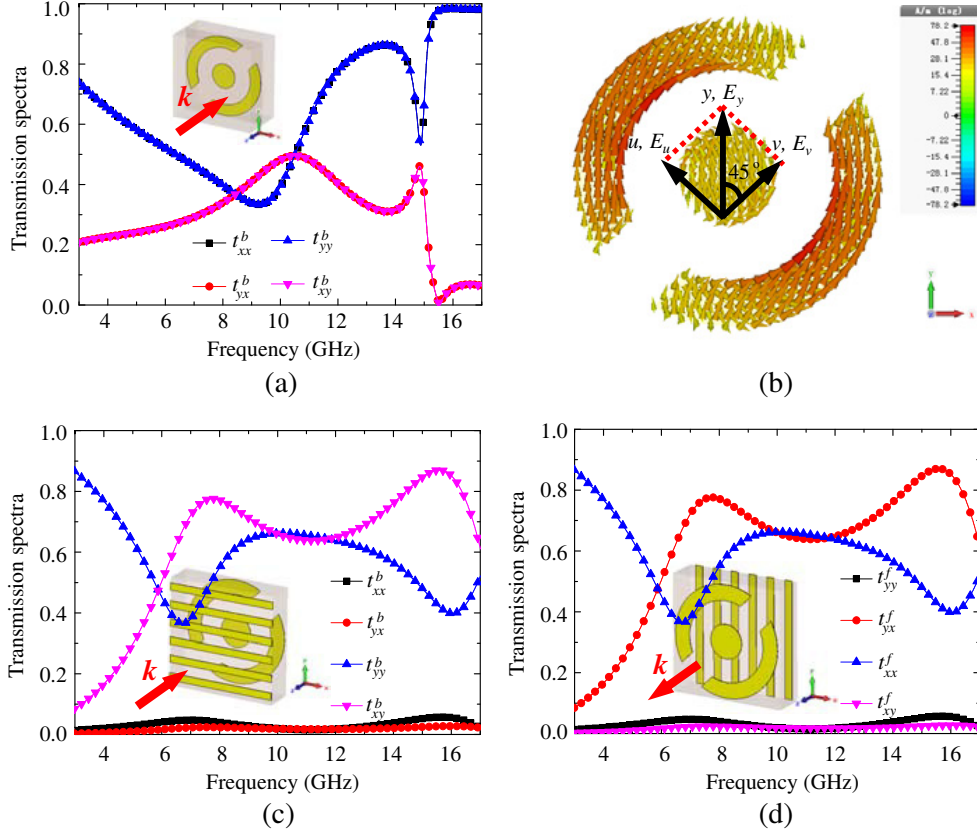
Figure 2. Simulated transmission coefficients of the (a) layer B, (c) bi-layer AB and (d) bi-layer BC, (b) surface current distributions of the DSRs for the incident y-polarized wave along backward $(-z)$ direction at 10.51 GHz.

its mechanism of this polarization conversion behavior, we simulated the surface current distribution of the DSRs for the incident y-polarized waves along backward $(-z)$ direction at 10.51 GHz, as shown in Fig. 2(b). We can find that the flow direction of surface current is rotated 45° along $x(y)$ axis, which forms electric dipolar resonances. As shown in the inset of Fig. 2(b), the incident y-polarized wave can be decomposed into two perpendicular components, u and v, respectively. At resonances, eigenmodes are excited only by v component of the electric field or u component of the incident y-polarized wave [49, 50]. For example, at 10.51 GHz, only v component of the electric field is excited by the incident y-polarized wave. Thus, the incident linearly polarized wave can only partially be converted to its orthogonal component at resonances. In fact, the DSRs will excite a dipolar oscillation along the split direction with two orthogonal components. One is along the $x(y)$-direction, and the other is along the $y(x)$ direction, finally resulting in a partial polarization conversion in transmission.

Figures 2(c) and (d) give the simulated transmission coefficients of the bi-layer AB and bi-layer BC, respectively, where the cross-polarization transmission t_{xy}^{b} and t_{yx}^{f} has been enhanced significantly in contrast to single layer B. As shown in Fig. 2(c), when the normal incident wave pass through the bi-layer AB along the backward $(-z)$ direction, t_{xx}^{b} and t_{yx}^{b} are nearly the same and close to zero across the whole frequency range, while t_{xy}^{b} is greater than 0.6 and t_{yy}^{b} below 0.6 in a broadband frequency range. It indicates that only y-polarized wave can pass through the bi-layer AB and partially converted into x-polarized wave in transmission, while the x-polarized wave is blocked extremely due to the polarization selection of layer A and the polarization conversion of layer B [44, 46, 47]. As shown in Fig. 2(d), when the normal incident wave pass through the bi-layer BC along the forward $(+z)$ direction, only x-polarized wave can pass through it and partially converted into y-polarized wave in transmission, while the y-polarized wave is blocked extremely. The bi-layer structures (AB and BC) can form a Fabry-

perot-like cavity, where the waves traveling back and forth between them can give birth to interference effect with the multiple polarization couplings, finally resulting in an enhanced CPC in a broadband frequency range [49–51]. From Figs. 2(c) and (d), it can be conjectured that the AT effect for linearly polarized waves can happen if combining layers A, B and C. It should be noticed that although the bi-layer structures (AB and BC) can realize the CPC in a broadband range, the efficiency is relatively low (the magnitude of the cross-polarization transmission is below 0.9).

According to the above analysis, the CPC efficiency and operation bandwidth could be enhanced significantly by adding a layer C to bi-layer AB forming a tri-layer ABC as shown in Fig. 1(d). To demonstrate the performance of the tri-layer structure of the CCMM, we present the simulated and measured transmission coefficients, respectively, as shown in Fig. 3. The experiment results are in qualitative agreement with the simulations, except for the slight discrepancies in the transmission magnitudes. These undesired deviations could be caused by the possible reasons including the fabrication imperfection and tiny distortion of the CCMM slab, and the finite dimensions of the sample in the experiment but not the simulation. Figs. 3(a) and (c) show the simulated and measured transmission spectra for the normal incident waves propagation along backward $(-z)$ direction, respectively. It can be seen that the co-polarization transmission coefficients t_{xx}^{b} of incident x-polarized wave and t_{yy}^{b} of incident y-polarized wave are exactly the same with each other, and both of them are less than 0.037 in the frequency range of 4.36–14.91 GHz. Nevertheless, the cross-polarization transmission coefficients
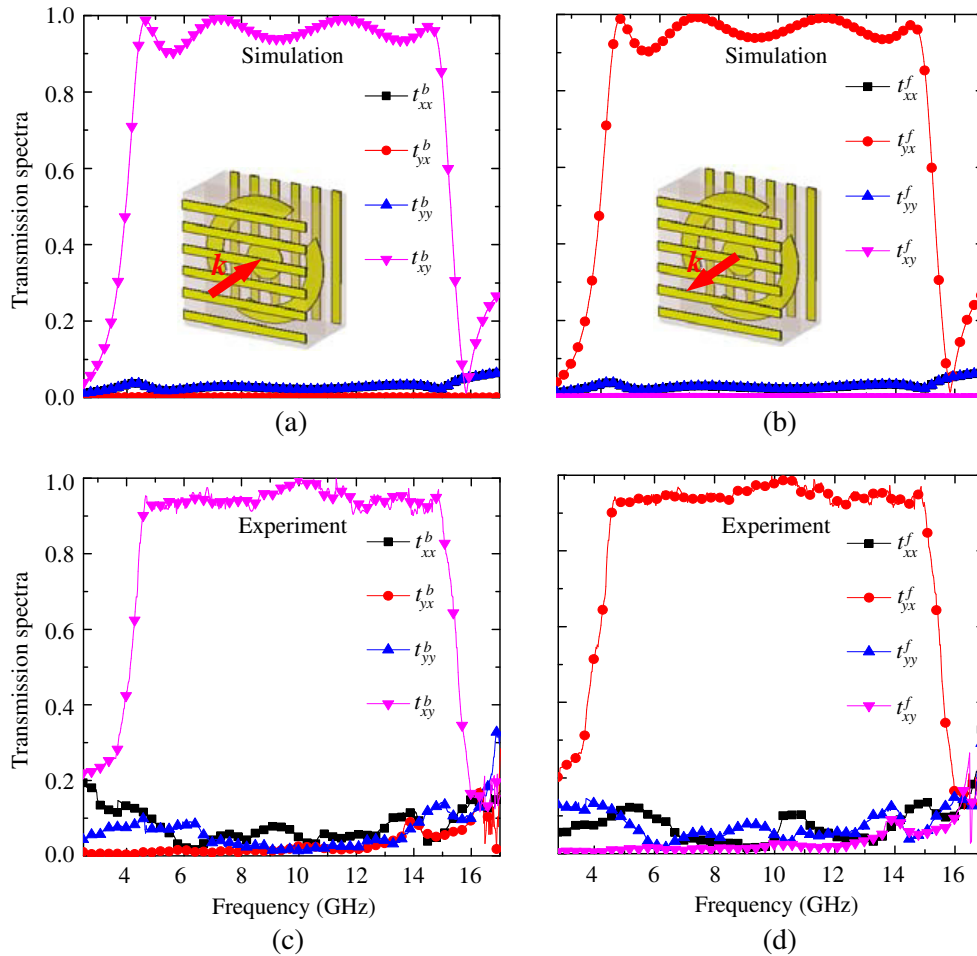
Figure 3. (a), (b) Simulated and (c), (d) experimental results: transmission coefficients $(t_{xx}^{f(b)}, t_{yx}^{f(b)}, t_{xy}^{f(b)}$ and $t_{yy}^{f(b)})$ for the normal incident waves passing through the CCMM along (a), (c) backward $(-z)$ direction (b), (d) forward $(+z)$ direction.

t_{xy}^b of incident y-polarized wave and t_{yx}^b of incident x-polarized wave are different remarkably. When the waves propagate along the backward $(-z)$ direction, t_{yx}^b is near zero across the whole frequency range while t_{xy}^b for the y-polarized wave is greater than 0.9 within the frequency range of 4.36–14.91 GHz corresponding to a relative bandwidth of about 104.49%. In addition, the maximal values of t_{xy}^b are up to 0.99 at 4.67 GHz, 7.24 GHz, and 11.57 GHz, respectively. Similar to the Fabry-Perot-like resonances, the near unity transmission of the cross-polarized wave t_{xy}^b can be achieved owing to the interference effect between the multiple polarization couplings of the waves transmission and reflection in the tri-layer structure [42–47, 49–51]. It indicates that the proposed CCMM can only realize a high-efficiency CPC for the incident y-polarized waves propagation along backward $(-z)$ direction. Figs. 3(b) and (d) present the transmission spectra for the forward $(+z)$ propagating waves. t_{xy}^b and t_{yx}^f of cross-polarization interchange with each other, and t_{xx}^b, t_{yy}^b, t_{xx}^f and t_{yy}^f of co-polarization are consistent when the propagation direction is reversed. In contrary to the results in Figs. 3(a) and (c), the proposed CCMM can only accomplish a high-efficiency CPC for the incident x-polarized waves (see Figs. 3(b), (d)). Compared with the single layer B, bi-layer AB and BC structures, the operation bandwidth and CPC efficiency have been improved significantly through this tri-layer structure of the proposed CCMM. Thus, it can be expected that the proposed CCMM slab can be used as a transparent ultra-broadband cross-polarization convertor. This distinct high-efficient CPC for the reversed propagation directions via remarkable AT effect is mainly attributed to the special structure chirality of the CCMM [51–53]. These results imply that the proposed CCMM can achieve giant AT effect for normal incident linearly polarized waves.

To clearly characterize the AT effect, the AT coefficients (Δ_{lin}) for simulation and measurement were calculated as shown in Fig. 4, and the calculation equations are detailed in [15, 16]. To guarantee the giant AT effect of the normal incident linearly polarized waves for the proposed CCMM, the cross-polarization transmission coefficients $(t_{yx}^{f(b)}$ and $t_{xy}^{f(b)})$ propagation along the opposite direction are also different which should be satisfied as [15, 16]: $\Delta_{lin}^{x,f(b)} = |t_{yx}^{f(b)}|^2 - |t_{xy}^{f(b)}|^2 = -\Delta_{lin}^{y,f(b)} \neq 0$. It is observed clearly that two curves of Δ_{lin}^x and Δ_{lin}^y are exactly the opposite, and their absolute values are equal and greater than 0.8 in an ultrabroadband range from 4.36 to 14.91 GHz. In addition, the magnitudes of the AT coefficients are greater than 0.95 at resonance frequencies. The measurements agree well with the simulations in principle. It should be noticed that the AT coefficients for circular polarization are kept to zero (not shown). Thus, the proposed CCMM only exhibits significant AT effect for the linearly polarized waves, but not for the circular polarizations. It is also noteworthy that the AT effect with simultaneous high amplitude and ultrabroadband has been realized experimentally using the tri-layer structure CCMM, which is very comparable with previous reported CMMs [29–38, 42–48].

To further characterize the AT effect, we calculated the total transmittance (T_y) of transmitted
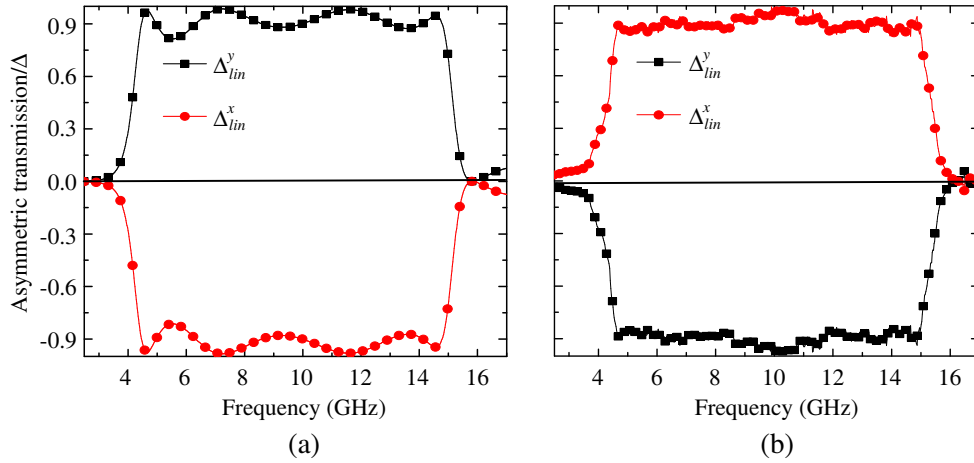
Figure 4. The (a) simulated and (b) experimental AT coefficients (Δ_{lin}).

x-polarized waves for both x-polarized and y-polarized incident waves along the forward $(+z)$ and backward (z) directions. The total transmittance of wave propagation along the forward and backward directions for x polarization and y polarization can be defined as [47]: $T_x^{f(b)} = |t_{xx}^{f(b)}|^2 + |t_{xy}^{f(b)}|^2$ and $T_y^{f(b)} = |t_{yy}^{f(b)}|^2 + |t_{yx}^{f(b)}|^2$, respectively. Figs. 5(a), (b) present the calculated total transmittance (T_x) of simulation and measurement, respectively. It is obvious that the total transmittance (T_x) of the waves propagation along the backward $(-z)$ direction is extremely different from that along the forward $(+z)$ direction. In both simulation and experiment, the total transmittance (T_x) of the x-polarized wave is greater than 0.8 for the backward $(-z)$ direction in an ultrabroadband range from 4.36 to 14.91 GHz, while it is near zero for the forward $(+z)$ direction. Therefore, it is further confirmed that the CCMM can realize AT effect, which is similar to a diode-like effect in an ultrabroadband range.

Furthermore, we calculated the PCR of x-polarized wave propagation along the forward $(+z)$ direction and y-polarized wave propagation along the backward $(-z)$ direction, respectively, and the calculation equations are detailed in [47]. Figs. 6(a), (b) display the calculated PCRs for simulation
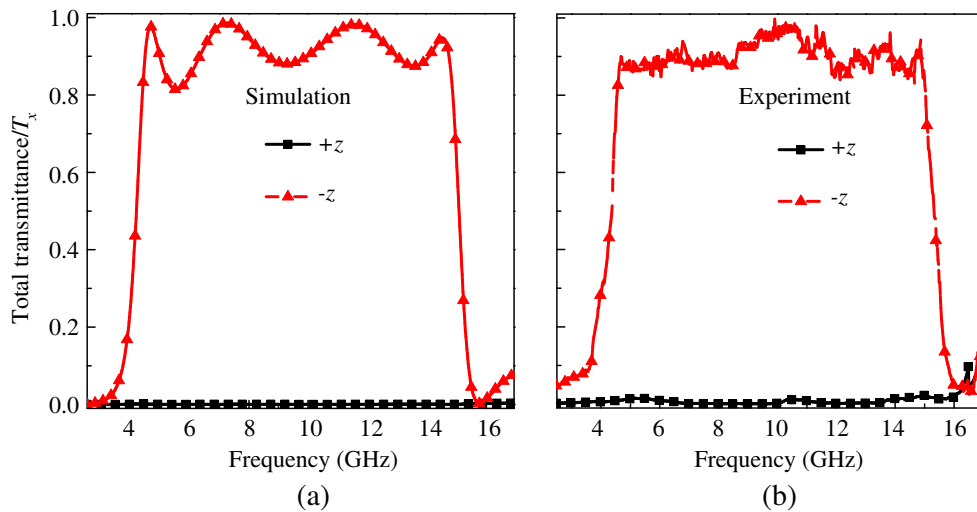
Figure 5. (a) The simulated and (b) experimental total transmittance (T_y) of transmitted x-polarized waves for both the x-polarized and y-polarized incident waves propagation along forward $(+z)$ and backward $(-z)$ direction.
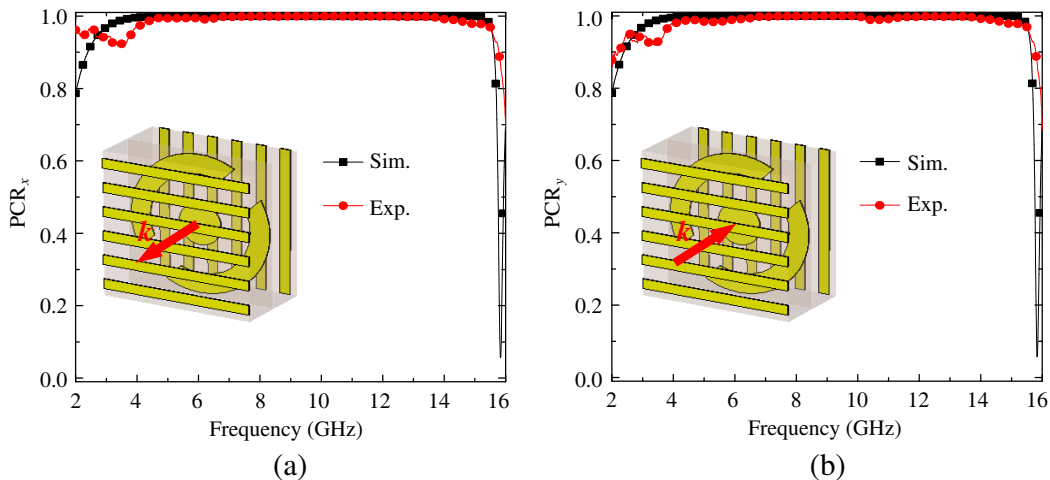
Figure 6. The simulated and measured results: PCR for (a) the x-polarized wave propagation along the forward $(+z)$ direction, and (b) the y-polarized wave propagation along the backward $(-z)$ direction.

and measurement, respectively. It can be seen that the PCR of x-polarized wave propagation along the forward $(+z)$ and y-polarized wave propagation along the backward $(-z)$ direction are consistent, and both of them always keep high magnitude of about 0.99 in an ultrabroadband frequency range. It should be noticed that the PCRs of y-polarized wave along $+z$ direction and x-polarized wave along $-z$ direction are also consistent, but both of them will always be kept near zero across the whole frequency range (not shown). Thus, our designed CCMM slab has a nearly perfect CPC capability in an ultrabroadband frequency range.

The conversion between x-polarized and y-polarized waves plays an important role in enhancing the high CPC effect. Therefore, to gain better insight into the linear polarization rotation or conversion of the proposed CCMM slab, the polarization azimuth angle (θ) and ellipticity (η) for a y-polarized wave along the backward $(-z)$ direction were calculated, respectively, and the calculation equations are detailed in [52]. Fig. 7 gives the simulated polarization azimuth angle and ellipticity. It can be seen that the value of θ is close to $-90°$ in frequency ranges of 4.36–4.96 GHz and 10.77–14.98 GHz, and close to $90°$ in frequency range of 4.96–10.77 GHz, implying that the incident y-polarized wave is mostly transmitted to the x-polarized wave with different rotation directions $(-x$ and $+x$ directions$)$. It means that with respect to the incident wave propagation along the backward $(-z)$ direction, the polarization plane of the transmitted wave has a near $-90°$ rotation in frequency ranges of 4.36–4.96 GHz and 10.77–14.98 GHz, and $+90°$ rotation in frequency range of 4.96–10.77 GHz. It should be noticed that the θ of x-polarized wave along the backward $(-z)$ direction will be close to zero (not shown). Thereby, it can be applied to realize the approximate ultrabroadband $90°$ polarization rotator for the incident special polarization wave. In addition, the absolute value of η is below $3°$ in the entire frequency range, indicating that the transmitted waves have a relatively high purity of linear polarization. These results further illustrate that the CCMM can convert a linearly polarized wave to its cross-polarization within an ultrabroadband frequency range.
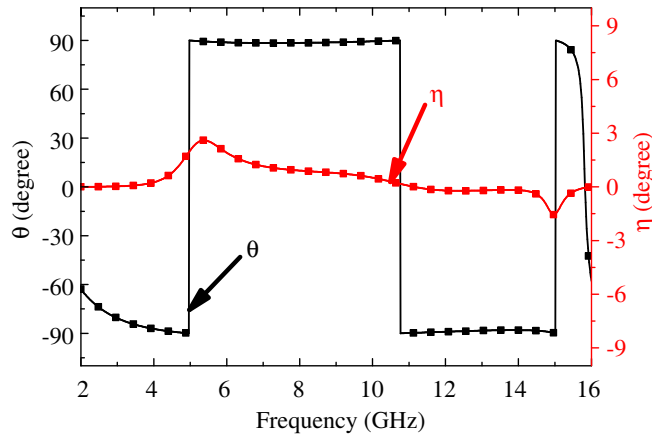
Figure 7. The simulated polarization azimuth rotation angle (θ) and polarization ellipticity angle (η) for the normal incident y-polarized wave propagation along the backward $(-z)$ direction.

In order to further illustrate the high-efficiency cross-polarization conversion and diode-like AT effect of the proposed CCMM, we also simulated and analyzed the electric fields distributions at different resonance frequencies. The AT effect and CPC effect can be visualized by electrical field distributions clearly. Fig. 8 present the visualized evolution process of electric fields in the x-z plane of the middle of unit-cell structure including incoming regime, substrate and the outgoing regime at $f_1 = 4.67$ GHz, $f_2 = 7.24$ GHz, and $f_3 = 11.57$ GHz, respectively.

As shown in Figs. 8(a1), (a3) and (c1), (c3), at 4.67 GHz and 11.57 GHz, the incident y-polarized $(+y$ direction$)$ and x-polarized $(+x$ direction$)$ waves propagation along backward $(-z)$ and forward $(+z)$ directions from the front and back metallic structures excite the guided resonant modes of the unit-cell structure and are finally perfectly converted to the transmitted x-polarized $(-x$ direction$)$ and y-polarized $(-y$ direction$)$ waves, respectively. At 7.24 GHz, as shown in Figs. 8(a2) and (c2), the incident
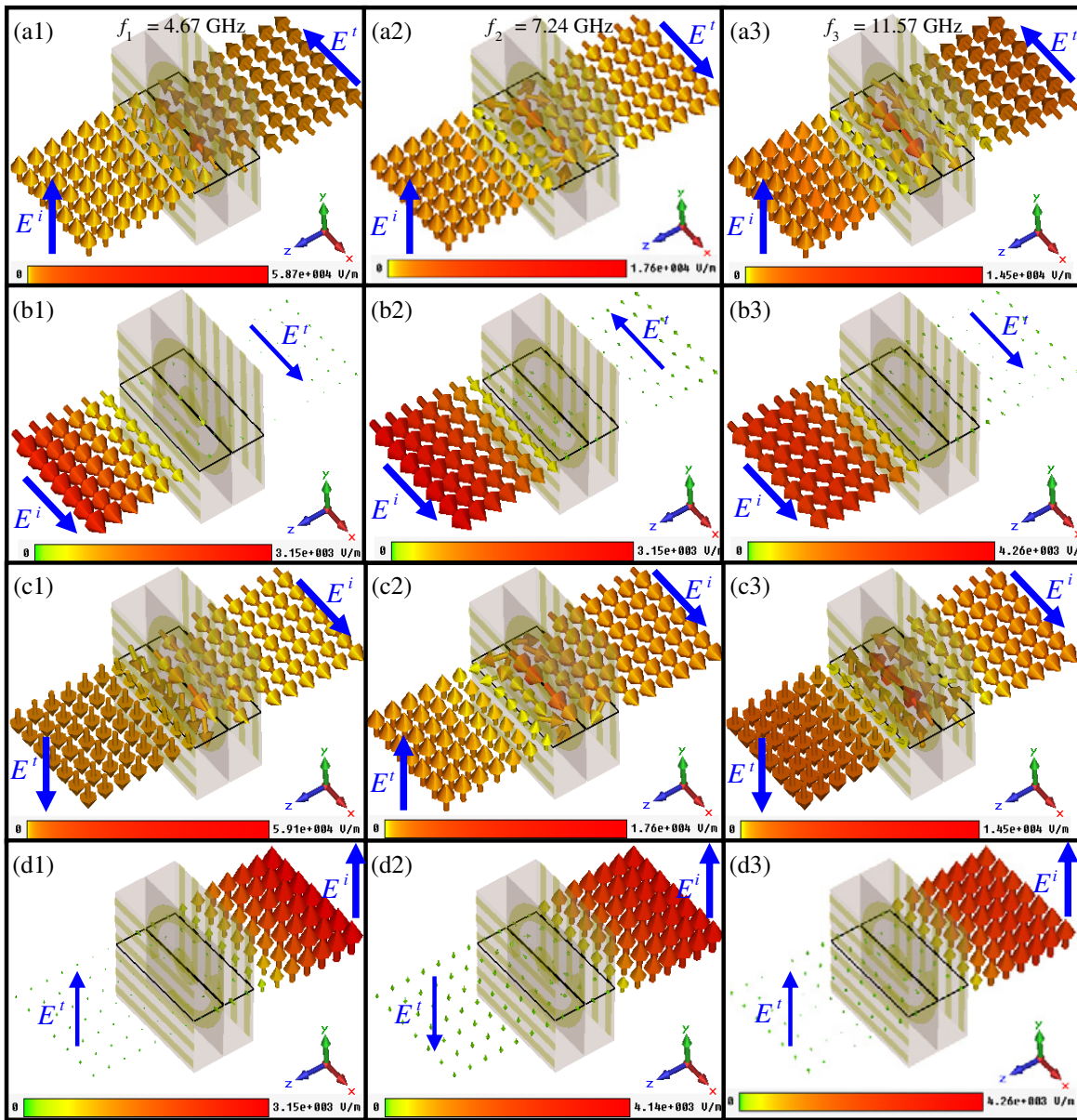
Figure 8. Simulated electric field distributions of the CCMM unit-cell structure in the x-z plane in case of the incident (a1)–(a3) y-polarized and (b1)–(b3) x-polarized wave along backward ($-z$) direction, and (c1)–(c3) x-polarized and (d1)–(d3) y-polarized wave along forward ($+z$) direction at different resonance frequencies: (a1)–(d1) $f_1 = 4.67$ GHz, (a2)–(d2) $f_2 = 7.24$ GHz, (a3)–(d3) $f_3 = 11.57$ GHz.

y-polarized ($+y$ direction) and x-polarized ($+x$ direction) waves propagation along backward ($-z$) and forward ($+z$) direction are finally perfectly converted to the transmitted x-polarized ($+x$ direction) and y-polarized ($+y$ direction) waves, respectively. As shown in Figs. 8(b1)–(b3) and (d1)–(d3), the incident x-polarized ($+x$ direction) waves and y-polarized ($+y$ direction) waves propagation along backward ($-z$) and forward ($+z$) direction are suppressed extremely at the entrances at above resonance frequencies, resulting in a very low transmission without polarization conversion. These results further imply that when the waves are propagating along the backward ($-z$) direction, only the y-polarized waves can be selected to pass through the CCMM slab and finally converted to the transmitted x-polarized waves while the x-polarized waves cannot allow to be transmitted. When propagation direction of the incident

wave is reversed, only the x-polarized waves can be selected and converted to the y-polarized waves, and the y-polarized waves cannot. In effect, all the fields patterns will be twisted inside the unit-cell structure as a consequence of interlayer interference coupling effect at these resonance frequencies [42–47, 49–51]. These electric field distributions pictures of unit-cell structure are in excellent consistency with the results in Figs. 4–7. The field distributions explicitly indicate that the excitation of local resonant modes and interlayer coupling in the tri-layer ABC structure are crucial to the ultrabroadband AT effect and CPC functionality, which is similar to the previous designed structures [42–47, 49–51]. These features of electric field distributions of unit-cell structure also further confirm that the CCMM could be served as an ultrabroadband 90° polarization rotator or cross-polarization convertor.

4. CONCLUSION

In conclusion, we propose a CCMM with the DSRs sandwiched between two layers of twisted sub-wavelength metal grating, which can realize an ultrabroadband AT effect and high-efficient CPC in microwave region. Both simulation and experiment reveal that the cross-polarization transmission coefficients (t_{xy}^b and t_{yx}^f) over 0.9 of the proposed CCMM can be realized from 4.36–14.91 GHz, corresponding to a relative bandwidth of about 104.49%, which are much larger than previous CMMs [29–38, 42–48]. Meanwhile, it also exhibits CPC with nearly 99% efficiency and approximately ±90° polarization rotation at above frequency range. Thus, our design can be functioned as an ultrabroadband linear polarization convertor or rotator. The whole thickness our design is about 5.1 mm, which is thinner than the previous proposed CMMs convertor or rotator [42–44]. The enhanced AT effect and high-efficient CPC of the proposed CCMM can be attributed to the Fabry-Pérot-like interference effect of cross coupling for the electric and magnetic fields [49–51]. In addition, owing to the geometry scalability, the proposed structure could operate well at terahertz and even optical region by scaling down the geometric dimensions. With the remarkable properties of ultrabroadband and high-efficiency, we believe that our proposed CCMM will be beneficial for designing circulator, isolator and polarization convertor or rotator.

REFERENCES

1. Lindelli, V., A. Sihvola, S. Tretyakov, et al., *Electromagnetic Waves in Chiral and Bi-isotropic Media*, Artech House, London, 1994.
2. Pendry, J. B., "A chiral route to negative refraction," *Science*, Vol. 306, 1353–1355, 2004.
3. Plum, E., J. Zhou, J. Dong, V. A. Fedotov, T. Koschny, C. M. Soukoulis, and N. I. Zheludev, "Metamaterial with negative index due to chirality," *Phys. Rev. B*, Vol. 79, No. 3, 035407, 2009.
4. Monzon, C. and D. W. Forester, "Negative refraction and focusing of circularly polarize waves in optically active media," *Phys. Rev. Lett.*, Vol. 95, 123904, 2005.
5. Li, J., F.-Q. Yang, and J.-F. Dong, "Design and simulation of L-shaped chiral negative refractive index structure," *Progress In Electromagnetics Research*, Vol. 116, 395–408, 2011.
6. Li, Z., K. B. Alici, E. Colak, and E. Ozbay, "Complementary chiral metamaterials with giant optical activity and negative refractive index," *Appl. Phys. Lett.*, Vol. 98, 161907, 2011.
7. Cheng, Y., Y. Nie, and R. Z. Gong, "Giant optical activity and negative refractive index using complementary U-shaped structure assembly," *Progress In Electromagnetics Research M*, Vol. 25, 239–253, 2012.

8. Cheng, Y., Y. Nie, L. Wu, and R. Z. Gong, "Giant circular dichroism and negative refractive index of chiral metamaterial based on split-ring resonators," *Progress In Electromagnetics Research*, Vol. 138, 421–432, 2013.

9. Decker, M., R. Zhao, C. M. Soukoulis, S. Linden, and M. Wegener, "Twisted split-ring-resonator photonic metamaterial with huge optical activity," *Opt. Lett.*, Vol. 35, No. 10, 1593–1593, 2010.

10. Kwon, D. H., P. L. Werner, and D. H. Werner, "Optical planar chiral metamaterial designs for strong circular dichroism and polarization rotation," *Opt. Express*, Vol. 16, No. 16, 11802–11807, 2008.

11. Fedotov, V. A., P. L. Mladyonov, S. L. Prosvirnin, A. V. Rogacheva, Y. Chen, and N. I. Zheludev, "Asymmetric propagation of electromagnetic waves through a planar chiral structure," *Phys. Rev. Lett.*, Vol. 97, No. 16, 167401, 2006.

12. Fedotov, V. A., A. S. Schwanecke, N. I. Zheludev, V. V. Khardikov, and S. L. Prosvirnin, "Asymmetric transmission of light and enantiomerically sensitive plasmon resonance in planar chiral nanostructures," *Nano Lett.*, Vol. 7, No. 7, 1996–1999, 2007.

13. Singh, R., E. Plum, C. Menzel, C. Rockstuhl, A. K. Azad, R. A. Cheville, F. Lederer, W. Zhang, and N. I. Zheludev, "Terahertz metamaterial with asymmetric transmission," *Phys. Rev. B*, Vol. 80, No. 15, 153104(5), 2009.

14. Menzel, C., C. Rockstuhl, and F. Lederer, "Advanced Jones calculus for the classification of periodic metamaterials," *Phys. Rev. A*, Vol. 82, 053811, 2010.

15. Huang, C., Y. Feng, J. Zhao, Z. Wang, and T. Jiang, "Asymmetric electromagnetic wave transmission of linear polarization via polarization conversion through chiral metamaterial structures," *Phys. Rev. B*, Vol. 85, No. 19, 195131, 2012.

16. Cheng, Y., Y. Nie, X. Wang, and R. Gong, "An ultrathin transparent metamaterial polarization transformer based on a twist-split-ring resonator," *Appl. Phys. A*, Vol. 111, 209–215, 2013.

17. Cong, L., W. Cao, X. Zhang, Z. Tian, J. Gu, R. Singh, J. Han, and W. Zhang, "A perfect metamaterial polarization rotator," *Appl. Phys. Lett.*, Vol. 103, No. 17, 171107, 2013.

18. Cheng, Y. Z., Y. Nie, Z. Z. Cheng, L. Wu, X. Wang, and R. Z. Gong, "Broadband transparent metamaterial linear polarization transformer based on triple-split-ring resonators," *Journal of Electromagnetic Waves and Applications*, Vol. 27, 1850–1858, 2013.

19. Wei, Z., Y. Cao, Y. Fan, X. Yu, and H. Li, "Broadband polarization transformation via enhanced asymmetric transmission through arrays of twisted complementary split-ring resonators," *Appl. Phys. Lett.*, Vol. 99, No. 22, 21907-3, 2011.

20. Han, J., H. Li, Y. Fan, Z. Wei, C. Wu, Y. Cao, X. Yu, F. Li, and Z. Wang, "An ultrathin twist-structure polarization transformer based on fish-scale metallic wires," *Appl. Phys. Lett.*, Vol. 98, No. 15, 151908, 2011.

21. Ma, X., C. Huang, M. Pu, C. Hu, Q. Feng, and X. Luo, "Multi-band circular polarizer using planar spiral metamaterial structure," *Opt. Express*, Vol. 20, No. 14, 16050–16058, 2012.

22. Song, K., X. Zhao, Y. Liu, Q. Fu, and C. Luo, "A frequency-tunable 90-polarization rotation device using composite chiral metamaterials," *Appl. Phys. Lett.*, Vol. 103, 101908, 2013.

23. Xu, H.-X., G.-M. Wang, M.-Q. Qi, and T. Cai, "Dual-band circular polarizer and asymmetric spectrum filter using ultrathin compact chiral metamaterial," *Progress In Electromagnetics Research*, Vol. 143, 243–261, 2013.

24. Wu, L., Z. Yang, Y. Cheng, R. Gong, M. Zhao, Y. Zheng, J. Duan, and X. Yuan, "Circular polarization converters based on bi-layered asymmetrical split ring metamaterials," *Appl. Phys. A*, Vol. 116, No. 2, 643–648, 2014.

25. Yogesh, N. F., T. Lan, and F. Ouyang, "Far-infrared circular polarization and polarization filtering based on Fermat's spiral chiral metamaterial," *IEEE Photonics Journal*, Vol. 7, No. 3, 1–12, 2015.

26. Ma, X., Z. Xiao, and D. Liu, "Dual-band cross polarization converter in bi layered complementary chiral metamaterial," *Journal of Modern Optics*, Vol. 63, No. 10, 937–940, 2016.

27. Tang, J., Z. Xiao, K. Xu, X. Ma, D. Liu, and Z. Wang, "Cross polarization conversion based on a new chiral spiral slot structure in THz region," *Opt. Quant. Electron.*, Vol. 48, 111, 2016.

28. Xu, K.-K., Z.-Y. Xiao, J.-Y. Tang, D.-J. Liu, and Z.-H. Wang, "Ultra-broad band and dual-band highly efficient polarization conversion based on the three-layered chiral structure," *Physica E*, Vol. 81, 169–176, 2016.

29. Menzel, C., C. Helgert, C. Rockstuhl, E.-B. Kley, A. Tunnermann, T. Pertsch, and F. Lederer, "Asymmetric transmission of linearly polarized light at optical metamaterials," *Phys. Rev. Lett.*, Vol. 104, 253902, 2010.

30. Kang, M., J. Chen, H. Cui, Y. Li, and H. Wang, "Asymmetric transmission for linearly polarized electromagnetic radiation," *Opt. Express*, Vol. 19, 8347, 2011.

31. Mutlu, M., A. E. Akosman, A. E. Serebryannikov, and E. Ozbay, "Asymmetric transmission of linearly polarized waves and polarization angle dependent wave rotation using a chiral metamaterial," *Opt. Express*, Vol. 19, 14290-9, 2011.

32. Novitsky, A. V., V. M. Galynsky, et al., "Asymmetric transmission in planar chiral split-ring metamaterials: Microscopic Lorentz-theory approach," *Phys. Rev. B*, Vol. 86, No. 7, 075138, 2012.

33. Mutlu, M., A. E. Akosman, A. E. Serebryannikov, and E. Ozbay, "Diodelike asymmetric transmission of linearly polarized waves using magnetoelectric coupling and electromagnetic wave tunneling," *Phys. Rev. Lett.*, Vol. 108, 213905, 2012.

34. Shi, J. H., X. C. Liu, S. W. Yu, T. T. Lv, Z. Zhu, H. F. Ma, and T. J. Cui, "Dual-band asymmetric transmission of linear polarization in bilayered chiral metamaterial," *Appl. Phys. Lett.*, Vol. 102, 191905, 2013.

35. Xu, Y., Q. Shi, Z. Zhu, and J. Shi, "Mutual conversion and asymmetric transmission of linearly polarized light in bilayered chiral metamaterial," *Opt. Express*, Vol. 22, No. 21, 25679–25688, 2014.

36. Han, S., H. Yang, L. Guo, X. Huang, and B. Xiao, "Manipulating linearly polarized electromagnetic waves using the asymmetric transmission effect of planar chiral metamaterials," *J. Opt.*, Vol. 16, No. 3, 035105, 2014.

37. Zhou, Z. and H. Yang, "Triple-band asymmetric transmission of linear polarization with deformed S-shape bilayer chiral metamaterial," *Appl. Phys. A*, Vol. 119, No. 1, 115–119, 2015.

38. Wang, Y. H., J. Shao, J. Li, Z. Liu, J. Li, Z. G. Dong, and Y. Zhai, "Broadband high-efficiency transmission asymmetry by a chiral bilayer bar metastructure," *J. Appl. Phys.*, Vol. 117, No. 17, 173102, 2015.

39. Liu, D., Z. Xiao, X. Ma, and Z. Wang, "Asymmetric transmission of linearly and circularly polarized waves in metamaterial due to symmetry-breaking," *Appl. Phys. Express*, Vol. 8, No. 5, 052001, 2015.

40. Wang, C., D. F. Tang, J. F. Dong, M. H. Li, and W. K. Pan, "Broad dual-band asymmetric transmission of circular polarized waves in near-infrared communication band," *Opt. Express*, Vol. 25, No. 10, 11329–11339, 2017.

41. Ji, R., S. W. Wang, X. Liu, and W. Lu, "Giant and broadband circular asymmetric transmission based on two cascading polarization conversion cavities," *Nanoscale*, Vol. 8, No. 15, 8189–8194, 2016.

42. Liu, D. Y., M. H. Li, X. M. Zhai, L. F. Yao, and J. F. Dong, "Enhanced asymmetric transmission due to fabry-perot-like cavity," *Opt. Express*, Vol. 22, 11707–11712, 2014.

43. Xiao, Z.-Y., D.-J. Liu, X.-L. Ma, and Z.-H. Wang, "Multi-band transmissions of chiral metamaterials based on Fabry-Perot like resonators," *Opt. Express*, Vol. 23, No. 6, 7053–7061, 2015.

44. Liu, Y., S. Xia, H. Shi, A. Zhang, and Z. Xu, "Efficient dual-band asymmetric transmission of linearly polarized wave using a chiral metamaterial," *Progress In Electromagnetics Research C*, Vol. 73, 55–64, 2017.

45. Shang, X.-J., X. Zhai, L.-L. Wang, M.-D. He, Q. Li, X. Luo, and H.-G. Duan, "Asymmetric transmission and polarization conversion of linearly polarized waves with bilayer L-shaped metasurfaces," *Appl. Phys. Express*, Vol. 10, 052602, 2017.

46. Wang, H.-B., X. Zhou, D.-F. Tang, and J.-F. Dong, "Diode-like broadband asymmetric transmission of linearly polarized waves based on Fabry-Perot-like resonators," *Journal of Modern Optics*, Vol. 7, 1–10, 2017.

47. Cheng, Y., R. Gong, and L. Wu, "Ultra-broadband linear polarization conversion via diode-like asymmetric transmission with composite metamaterial for terahertz waves," *Plasmonics*, Vol. 12, 1113–1120, 2016.

48. Huang, X., B. Xiao, D. Yang, and H. Yang, "Ultra-broadband 90° polarization rotator based on bi-anisotropic metamaterial," *Optics Communications*, Vol. 338, 416–421, Mar. 1, 2015.

49. Cheng, Y., W. Withayachumnankul, A. Upadhyay, H. Daniel, Y. Nie, R. Gong, M. Bhaskaran, S. Sriram, and D. Abbott, "Ultra-broadband reflective polarization convertor for terahertz waves," *Appl. Phys. Lett.*, Vol. 105, No. 19, 181111, 2014.

50. Zhao, J. and Y. Cheng, "A high-efficiency and broadband reflective 90° linear polarization rotator based on anisotropic metamaterial," *Appl. Phys. B*, Vol. 122, No. 10, 255, 2016.

51. Grady, N. K., J. E. Heyes, D. R. Chowdhury, Y. Zeng, M. T. Reiten, A. K. Azad, A. J. Taylor, D. A. Dalvit, and H. T. Chen, "Terahertz metamaterials for linear polarization conversion and anomalous refraction," *Science*, Vol. 340, No. 6138, 1304–1307, 2013.

52. Cheng, Y., C. Wu, Z. Z. Cheng, and R. Z. Gong, "Ultra-compact multi-band chiral metamaterial circular polarizer based on triple twisted split-ring resonator," *Progress In Electromagnetics Research*, Vol. 155, 105–113, 2016.

53. Song, K., Y. Liu, C. Luo, and X. Zhao, "High-efficiency broadband and multiband cross-polarization conversion using chiral metamaterial," *J. Phys. D: Appl. Phys.*, Vol. 47, 505104, 2014.